DALTON
FULL PAPER

Synthesis, $^1H/^{13}C$ NMR spectroscopic and structural studies of sterically induced internal dynamics in novel mono- and di-ruthenium(II) 2,2′:6′,2″-terpyridine complexes of 2,3-bis(2,2′-bipyridin-6-yl)pyrazine

Fenton R. Heirtzler,*[a] Markus Neuburger,[a] Margareta Zehnder,[a] Steven J. Bird,[b] Keith G. Orrell*[b] and Vladimir Sik[b]

[a] *Departement Chemie der Universität, Spitalstrasse 51, CH-4056 Basel, Switzerland*
[b] *Department of Chemistry, The University of Exeter, UK EX4 4QD*

Received 14th October 1998, Accepted 10th December 1998

The mono- and di-metallic N_6-ruthenium(II) complexes $[Ru(terpy)L][PF_6]_2$ **1** and $[\{Ru(terpy)\}_2L][PF_6]_4$ **2**, where L is 2,3-bis(2,2′-bipyridin-6-yl)pyrazine and terpy is 2,2′:6′,2″-terpyridine, have been prepared. Extensive and careful ^1H and ^{13}C NMR spectroscopic studies at ambient temperature showed that complexation induces steric strain in the scaffolding of L and thereby fluxional behaviour in both complexes. In **1**, rotation of the free 2,2′-bipyridyl (bpy) group of L relieves these interactions and results in two enantiomerically related conformations. In **2**, a mutual twisting of both complexed bpy fragments results in helicene-like, *P*- and *M*-configured enantiomeric complexes. Dynamic low-temperature NMR studies of **1** and **2** in acetone-d_6 solutions have provided activation energy data for both processes. The behaviour of **2** is paralleled by its crystal structure, which indicated a strong twisting of the bpy groups of L. Cyclic voltammetric and UV-spectroscopic studies conducted on both indicated a mild electrochemical and electronic coupling of the metal centres in **2**.

The synthesis and characterisation of di- and multi-metallic transition metal complexes with helical structures has been thoroughly explored over the past two decades. Helicates, which result from the self-assembly of two or more flexible ligand strands to wrap around metal centres,[1] and metallorganic structures analogous to helicenes,[2] in which complexation of a rigidly helical pre-organised ligand occurs, demonstrate two variations on this theme. The racemisation mechanisms of these two different types of complexes constitute a major difference between them. In the former, this generally occurs by exchange of labile metal–donor bonds with the surrounding medium, while interconversion of enantiomeric complexes of helicenes would require surmounting the steric barrier inherent in the ligand structure.[3,4] Expanded heterohelicenes which spontaneously form single- and double-helical complexes are also known,[5] as is a double-helical kinetically inert dimetallic complex.[6]

We are interested in the preparation[7] and metallosupramolecular complexes[8] of 2,3-bis(2,2′-oligopyridyl)pyrazines, and the availability of 2,3-bis[6-(2,2′-bipyridyl)]pyrazine **I** prompted our investigation of its corresponding dimetallic complexes with non-labile octahedral metal centres. The structure of **I** suggests that, upon bis-η^6 complexation, steric crowding around the pyrazine core of **I** would induce a helicene-like topology. In contrast to the aforementioned complexes of helicenes, the helicity of this substance would arise from complexation-induced allosteric interactions within the ligand scaffolding. This situation resembles that anticipated for the bis(2,2′-bipyridyl)ruthenium(II) complex of 2,3-bis(2-pyridyl)-pyrazine.[9] Here, however, the stereochemical ambiguity about the metal centres in that complex is circumvented by the bis-N_3-chelating nature of **I**. Several examples of complexes in which simple chirality is introduced by allosteric ligand interactions are already known.[10] Also of interest was the extent to which intermetallic communication would be perturbed by the steric strain inherent in such a dimetallic complex.

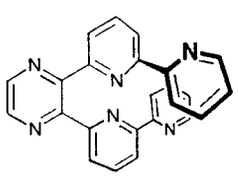

I

Results and discussion

Synthesis of ruthenium(II) complexes

Treatment of compound **I** with 1.1 equivalents of (2,2′:6′,2″-terpyridine)ruthenium(III) trichloride in boiling ethanol and in the presence of *N*-ethylmorpholine as reducing agent gave the monometallic complex **1** in 16% yield together with unchanged **I** after column chromatography and recrystallisation (see Scheme 1). After filtering through aluminium oxide to remove Ru^{III}-containing impurities, the only product which could be detected in the ^1H NMR spectrum of the crude material was **1**. This finding contrasts the tendency of other ligands having several terpy-like binding sites co-ordinatively to saturate with the largest possible number of ruthenium(II)–terpy fragments,[11–13] which has been postulated to arise from metal–ligand π-back-bonding activation of monoruthenium(II) complexes.[14] The behaviour of **I** may arise from both the reaction conditions and steric or electronic interactions in the transition state from **1** to the corresponding dimetallic complex (see below). Under more rigorous conditions [*e.g.* use of 2.4 equivalents of (2,2′:6′,2″-terpyridine)ruthenium(III) triacetonate[15]] and in analogy to literature precedent (*e.g.* refluxing *n*-butanol[16]) **I** afforded the diruthenium(II) complex **2** in 34% yield and starting material after chromatographic purification and recrystallisation. According to ^1H NMR spectroscopy, **2** was the only product present in the crude reaction mixture. Primary identification of **1** and **2** was from their time-of-flight (**1**) and FAB (**2**) mass

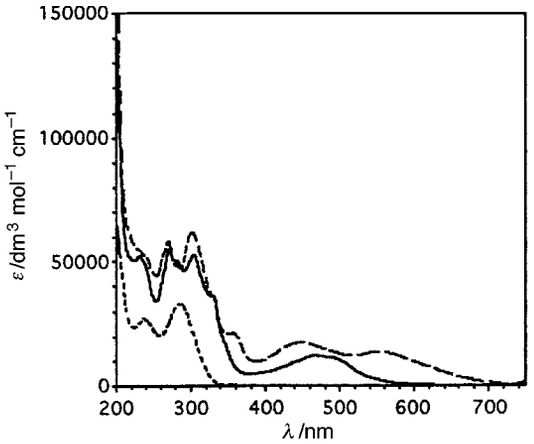

Fig. 1 Electronic spectra of compounds in MeCN: **1**, ——; **2**, – – –; **I**, - - - - -. Spectrum of **I** taken from ref. 7.

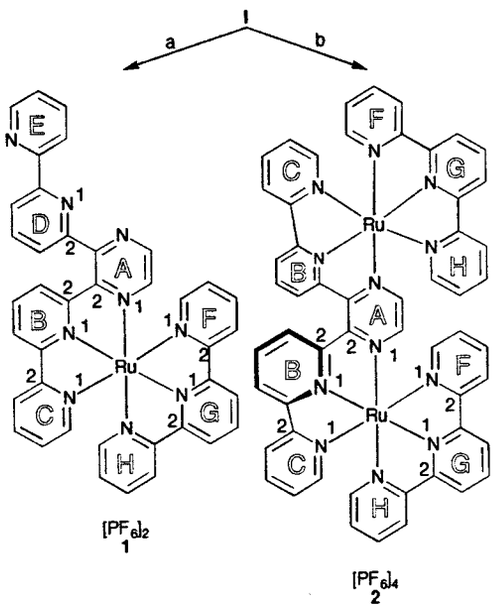

Scheme 1 Synthesis of the ruthenium(II) complexes. a, 1.1 equivalents [Ru(terpy)Cl_3], EtOH, *N*-ethylmorpholine, 4 h, then [NH_4][PF_6]; b, 2.4 equivalents Ru(terpy)Cl_3, 10 equivalents [Ag][BF_4], Me_2CO, reflux, 3h, then **I**, *n*-BuOH, reflux, 12 h, N_2 then [NH_4][PF_6].

spectra, which exhibited signals corresponding to the anticipated positive mass fragments.

Electronic and electrochemical characterisation

Initially, we considered the electronic spectra of complexes **1** and **2** in acetonitrile (see Fig. 1). In the UV region, the absorptions at 232 and 302/303 nm arise from ligand-based transitions of **I**, while those at 271/270 and 331 nm are characteristic of $Ru(terpy)_2^{2+}$.[17] Above *ca.* 400 nm the spectral profiles of **1** and **2** are dominated by broad MLCT transitions. For **1** a maximum at 467 nm and a shoulder at 490 nm are observed, which can be assigned to Ru ⟶ **I** and Ru ⟶ terpy π–π* transitions (or *vice versa*). For **2** the Ru ⟶ terpy transition occurs at 480 nm, blue shifted relative to that of **1**. The MLCT transition involving **I** is red-shifted to 555 nm, as would be expected upon stabilisation of its π* orbitals by complexation to a second metal center. Detailed studies on the luminescent and excited-state behaviour of **1** and **2** and related complexes will be undertaken in collaboration with an appropriate third party.

Cyclic voltammetric studies on both complexes also evidenced metal–ligand and intermetallic interactions. In the event of significant delocalisation over the scaffolding of compound **I**, then **2** should display two separate half-wave potentials for

Table 1 Cyclic voltammographic potentials of ruthenium complexes in acetonitrile solution[a]

	$E°$/V[ΔE_p[b]/mV]	
Complex	Oxidation	Reduction
1	1.44 [140]	−1.48 [200], −0.98 [140]
2	1.43 [80], 1.69 [120]	−1.84 [irrev.], −1.65 [100], −1.35 [140], −0.97 [irrev.], −0.57 [60]

[a] All potentials relative to the ferrocenium–ferrocene couple. [b] Difference between cathodic and anodic peak currents.

the Ru^{II}–Ru^{III} oxidative couple, and the magnitude of the difference between these potentials ($\Delta E°$) will be proportional to the strength of the interaction. In the positive potential region in acetonitrile the Ru^{II}–Ru^{III} couple of **1** exhibits one such half-wave, while **2** displays two, with the difference between them, $\Delta E° = 0.26$ V (Table 1). This value lies between those observed for the isomeric diruthenium(II) terpy complexes of 2,3,5,6-tetrakis(2-pyridyl)pyrazine **II**[13] and 4,6-bis(2,2′-bipyridyl)pyrimidine **III**[12] (0.31 and 0.16 V, respectively). This fact, and the closeness of the first Ru^{II}–Ru^{III} oxidation potentials observed for **1** and **2**, evidence moderate metal–metal interaction in **2**.

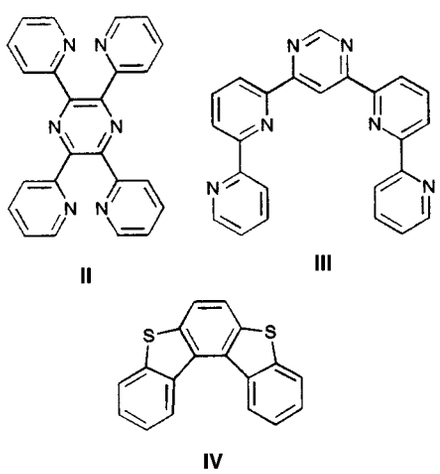

At negative potentials we observed ligand-based redox processes. For monometallic complex **1** two reversible ligand-based reductions occur. Control experiments indicated that free compound **I** is irreversibly reduced at −1.92 V. Since pyrazine-based **I** should be more readily reduced than the terpy ring system[18] we assign the least negative wave to the reduction of **I** and the second to terpy. The ligand-based electrochemical processes for dimetallic **2** were considerably more complicated, as its cyclic voltammogram displayed three reversible and at least two irreversible reductions. However, one of these occurred at a distinctly more positive potential than the other reduction potentials in **2** *and* **1**. As the binding of one, then two positively charged metal centers to **I** should render its reduction progressively more facile, this process is ascribed to **I**. The other two reversible processes are tentatively interpreted as terpy-based reductions. However, the fact that the differences between the ruthenium-based oxidation potentials and those terpy-based reduction voltages are greater in **1** than in **2** contrasts the trend expected from the blue-shifting of the Ru ⟶ terpy π–π* transition in the electronic spectrum of **2**.[19]

NMR spectroscopic studies

The room temperature ^{1}H NMR spectrum of the monometallic complex **1** in acetone-d_6 solution consisted of 22 multiplets, 5 being of double the intensity of the rest (Fig. 2). All signals were sharp, displayed the expected 3- and 4-bond H–H scalar

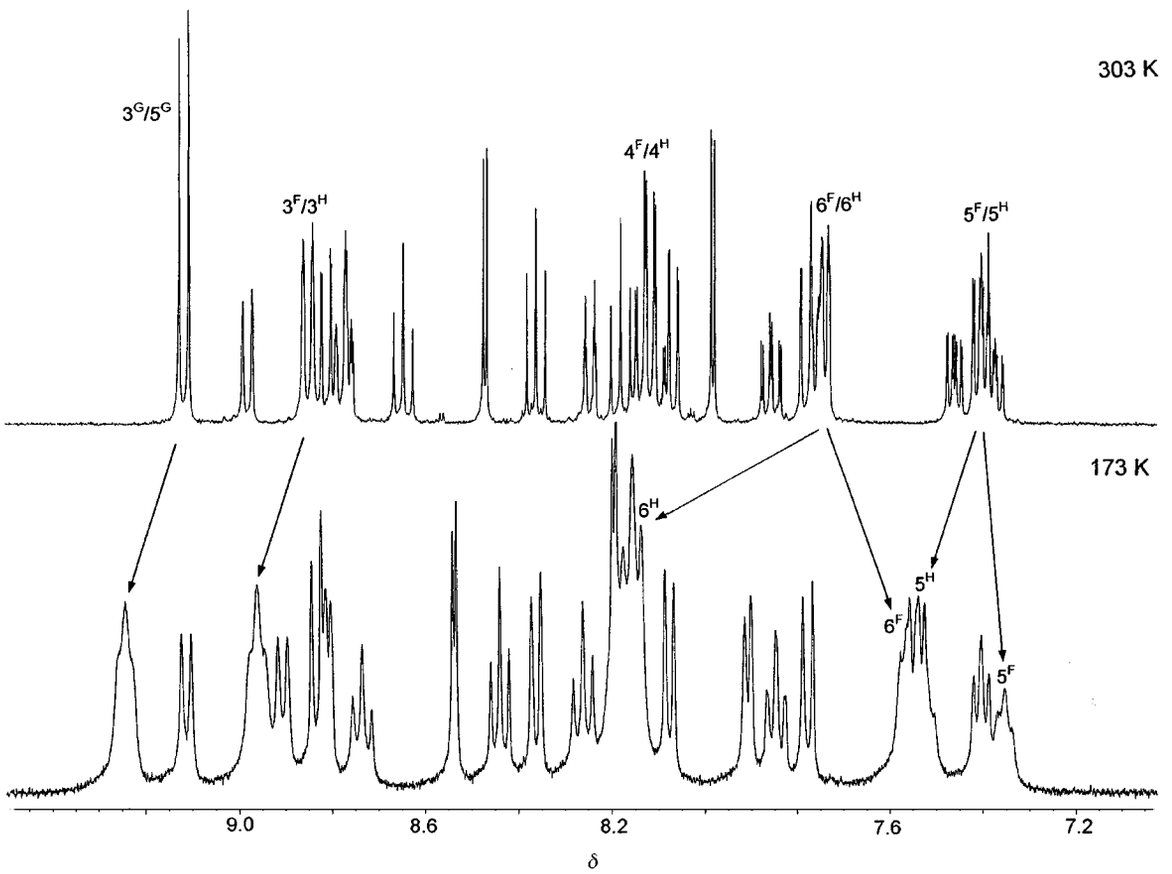

Fig. 2 The 400 MHz ^{1}H NMR spectra of complex **1** in $(CD_3)_2CO$ solution at 303 and 173 K.

couplings and were assigned with the aid of a COSY spectrum (Table 2). Assignment of the ^{13}C spectrum was based on ^{1}H–^{13}C correlation spectra, heteronuclear multiple quantum correlation (HMQC)-type[20] for 1-bond correlations and heteronuclear multiple bond correlations (HMBC)-type[21] for 2- and 3-bond correlations. The spectrum was composed of 31 resolved lines which, following a DEPT experiment, analysed as 22 methine carbons and 9 quaternary carbons. As the structure of **1** requires 22 methine and 10 quaternary carbons, one quaternary carbon, most likely the pyrazine carbon C(2^A), was undetectable. Overall, these results are consistent with a structure possessing a symmetry plane (σ) bisecting the central nitrogen of the terpy ring system.

Upon cooling, however, the double-intensity ^{1}H signals of the terpy rings in complex **1** changed notably. In particular, the multiplets associated with H(6^F/6^H) and H(5^F/5^H) broadened, passed through a coalescence region and eventually split into equal-intensity multiplets. This separation between the pairs of signals, $\Delta\delta$, was clearly detectable at 173 K (Fig. 2), especially for H(6^F/6^H) ($\Delta\delta$ 0.65), but also for H(5^F/5^H) ($\Delta\delta$ 0.20). The signals of H(3^F/3^H) and H(3^G/5^G) displayed similar effects but with much reduced splittings ($\Delta\delta$ 0.03 and 0.02 respectively). A slight change was detected in signal H(4^F/4^H) but signal overlaps prevented its accurate measurement.

These spectral changes of complex **1** are clearly associated with the arresting of a dynamic process which at room temperature is otherwise rapid. In particular, it is clear that this process must render the two sides of the terpy ring system non-equivalent and produce significant deshielding of the magnetic environments of terpy H(5^H) and H(6^H) compared to those at terpy H(5^F) and H(6^F). How this might occur was revealed by consideration of molecular models, which indicated severe steric interactions between pyridine rings "B" and "D". These effects can only be relieved through rotation of the non-complexing pendant bpy away from the plane of the pyrazine ring and into a flank of the terpy ring system. Thus, oscillation

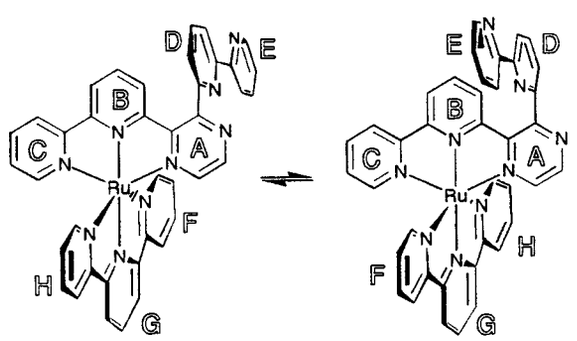

Fig. 3 Interconversion of enantiomeric rotamers of complex **1**.

of the bpy fragment between the two sides of the terpy ring system, to produce two mirror-image atropisomers, would account for the dynamic phenomenon (Fig. 3). Regardless of the actual conformational preferences of the pendant bpy, models show that this motion would cause significant through-space interactions between bpy ring "D" and terpy ring "H" which would completely account for the observed deshielding effects (*cf.* compound **2** later). Here, it is important to understand that the proximity of rings "B" and "D" undoubtedly results in steric interactions which are indeed greater than those between rings "D" and "H". However, it is the different magnitudes of interaction by bpy ring "D" with terpy rings "H" and "F" which allow NMR observation of the dynamic process. The terpy moiety is thus acting as a sensitive spectator ligand to the process caused by the interaction of the bpy "B" and "D" rings.

Whilst pyridyl ring rotations in metal complexes have been reported extensively,[22,23] to our knowledge the rotation of bpy moieties has not yet been documented. It was therefore of interest to confirm our hypothesis and measure the energy barrier for this dynamic process. However, strong signal over-

Table 2 Proton and ^{13}C NMR data of complex **1** in $(CD_3)_2CO$ solution at 303 and 173 K

Ring	Position	C[a]	H[a]	J_{HH}[a]/Hz	terpy splitting[b]
A	2	?	—		
	3	155.91	—		
	5	146.74	8.47	3.1	
	6	146.53	7.98	3.1	
B	2	155.75	—		
	3	128.70	7.78	8.2, 0.7	
	4	136.08	8.18	8.2, 8.2	
	5	124.93	8.98	8.2, 0.7	
	6	156.65	—		
C	2	159.03	—		
	3	125.47	8.78	8.2, 1.2, 0.7	
	4	139.67	8.11	8.2, 7.6, 1.5	
	5	128.84	7.37	7.6, 5.4, 1.2	
	6	153.09	7.76	5.4, 1.5, 0.7	
D	2	157.08	—		
	3	125.75	8.07	7.7, 1.0	
	4	140.32	8.36	8.2, 7.7	
	5	123.35	8.81	8.2, 1.0	
	6	155.50	—		
E	2	155.65	—		
	3	121.54	8.24	7.9, 1.2, 0.8	
	4	138.06	7.85	7.9, 7.4, 1.8	
	5	125.40	7.46	7.4, 4.8, 1.2	
	6	150.38	8.76	4.8, 1.8, 0.8	
F/H	2	159.11	—		
	3	125.69	8.85	8.0, 1.3, 0.7	8.98, 8.95
	4	139.59	8.12	8.0, 7.6, 1.5	minimal splitting
	5	128.78	7.40	7.6, 5.5, 1.3	7.55, 7.35
	6	153.57	7.74	5.5, 1.5, 0.7	8.20, 7.55
G	2	156.29	—		
	3	125.09	9.12	8.2	9.26, 9.24
	4	137.81	8.65	8.2, 8.2	
	5	125.09	9.12	8.2	9.26, 9.24
	6	156.29	—		

[a] At 303 K. [b] At 173 K.

Table 3 Activation energy data for the dynamic processes in compounds **1** and **2**

Compound	Process	$\Delta H^{\ddagger}$/ kJ mol^{-1}	$\Delta S^{\ddagger}$/ J K^{-1} mol^{-1}	$\Delta G^{\ddagger}$[a]/ kJ mol^{-1}
1	BR[b]	40.9 ± 1.4	15.8 ± 7.5	36.2 ± 0.8
2	RT[c]	56.1 ± 1.2[d]	12.7 ± 4.4[d]	52.3 ± 0.1[d]

[a] At 298.15 K. [b] bpy 180° rotation. [c] Racemisation twist. [d] Average value from bandshape analyses of both $6^F/6^H$ and $5^F/5^H$ regions.

lap, even under the initial conditions (*i.e.* 303 K), resulted in this being a non-trivial task, and demanded spectra of exceptional quality. Total bandshape analysis of signals $H(5^F)$ and $H(5^H)$ was performed at seven temperatures in the range 173–203 K. This analysis was complicated by *ortho*- and *meta*-ring couplings of these signals and overlap with the multiplets of signals $H(5^C)$, $H(5^E)$ and $H(6^F)$. Nevertheless, good agreement between experimental and computer simulated spectra was obtained (Fig. 4), from which reliable activation energy data for the restricted rotation were calculated (Table 3). The magnitude of the energy barrier ($\Delta G^{\ddagger}$) for this process resembles that observed for pyridyl rotation in $[ReCl(CO)_3(terpy)]$[23] (36.0 kJ mol^{-1}). This similarity may however be circumstantial, as **1** possesses considerably more degrees of freedom and undergoes different geometrical interactions than the rhenium(I) complex.

The ^1H NMR spectrum of dimetallic complex **2** at 303 K in $(CD_3)_2CO$ consisted of 14 chemically shifted signals, five of which were of double intensity, with one signal of this set being exceptionally broad, $\nu_{1/2} \approx 20$ Hz (Fig. 5). The spectrum was fully assigned (Table 4) with the aid of a COSY experiment. Its ^{13}C spectrum at 303 K comprised 20 signals (14 methine and 6 quaternary carbons, one somewhat broader than the rest) and was assigned by ^1H–^{13}C (HMQC and HMBC) correlation spectra in the same way as for compound **1**. These results are only consistent with a structure displaying C_{2v} symmetry, *i.e.* two symmetry planes which bisect the pyrazine ring and the terpy moieties, respectively at 303 K.

The broad ^1H and ^{13}C signals of complex **2** were due to $H(6^F/6^H)$ and $C(6^F/6^H)$ in the terpy ligands and indicated that a dynamic process was occurring which averaged two different environments for both sides of the terpy ligands. A series of proton spectra was therefore obtained in the low temperature range ambient to 203 K. Large scale changes occurred with the 5 double-intensity signals first broadening and then eventually splitting (to very variable extents) into equal-intensity pairs. The most extensive change occurred to signals $6^F/6^H$, where at low temperatures, $\Delta\delta$ was 1.36. The splittings of the other terpy signals decreased consistently around the ring, $\Delta\delta$ being 0.15 ($5^F/5^H$), 0.11 ($4^F/4^H$) and 0.04 ($3^F/3^H$). A very small (≈ 1 Hz) chemical shift distinction between the 3^G and 5^G hydrogens of the central terpy ring was also detectable. The proton spectra of **2** at 323, 253 and 203 K are shown in Fig. 5.

Inspection of models of complex **2** suggested an explanation for this behaviour, and illustrated how it differed from that of the mononuclear complex **1**. Steric repulsion between the pyridine "B" rings of ligand **I** should twist the bpy ring systems equally away form one another and out of the symmetry plane

Table 4 Proton and ^{13}C NMR data of complex **2** in $(CD_3)_2CO$ solution at 303 and 173 K

Ring	Position	C[a]	H[a]	J_{HH}[a]/Hz	terpy splitting[b]
A	2	155.98	—		
	3	155.98	—		
	5	148.76	7.45	—	
	6	148.76	7.45	—	
B	2	154.80	—		
	3	130.15	9.71	8.3	
	4	136.73	8.52	8.2, 8.2	
	5	126.83	9.17	8.2	
	6	157.28	—		
C	2	158.60	—		
	3	125.86	8.86	7.8, 1.2	
	4	140.13	8.13	7.7, 7.7, 1.4	
	5	129.01	7.34	7.8, 5.6, 1.3	
	6	153.30	7.72	5.6, 1.3	
F/H	2	158.75	—		
	3	125.66	8.66	7.9, 1.3	8.74, 8.70
	4	139.82	8.01	7.9, 7.9, 1.4	8.09, 7.98
	5	128.74	7.26	7.0, 5.6, 1.3	7.38, 7.23
	6	153.71	7.59	broad	8.34, 6.98
G	2	155.92	—		
	3	125.12	8.92	8.1	8.99[c]
	4	138.34	8.48	8.2, 8.2	
	5	125.12	8.92	8.2	8.99[c]
	6	155.92	—		

[a] At 303 K. [b] At 173 K. [c] Shifted to δ 8.99 and minimally split (≈ 1 Hz).

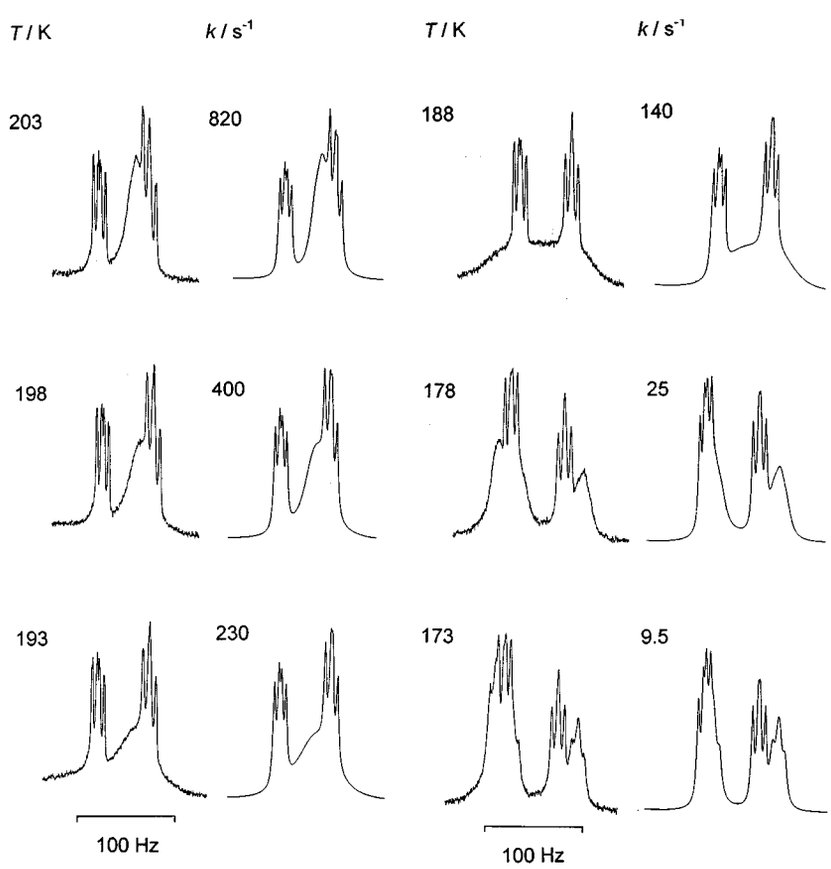

Fig. 4 Bandshape analyses of signals $H(5^F/5^H)$ of complex **1**, showing the best-fit rate constants. The spectator signals due to $H(5^C)$ and $H(5^E)$ were also included in the fittings. [At temperatures below ≈ 190 K the high frequency edge of experimental spectra includes signal $H(6^F)$ which was *not* included in the fittings.]

bisecting the terpy ring systems (Fig. 6). The stereochemical consequence of this distortion is for the terpy ligands to slip in opposite directions such as to disrupt the symmetry plane apparent at room temperature and which bisects the pyrazine ring. In the resulting structure the terpy ring systems adopt a staggered relationship in which their flanks (*i.e.* rings "F" and "H") become chemically non-equivalent. Magnetically equivalent flanks of the two terpy moieties are interrelated by the C_2

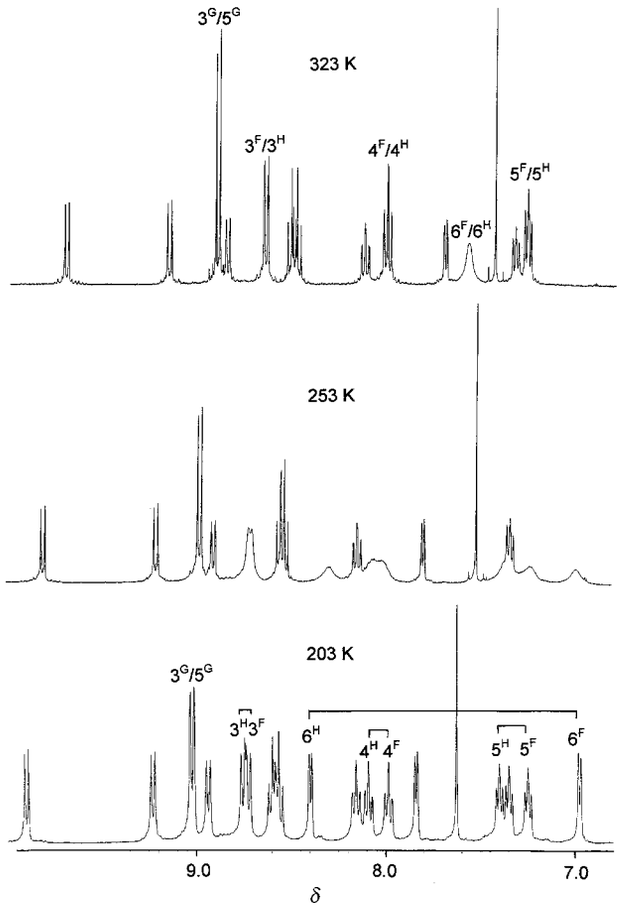

Fig. 5 The 400 MHz ^{1}H NMR spectra of complex **2** in $(CD_3)_2CO$ solution at 323, 253 and 203 K, showing the effects of the racemisation process.

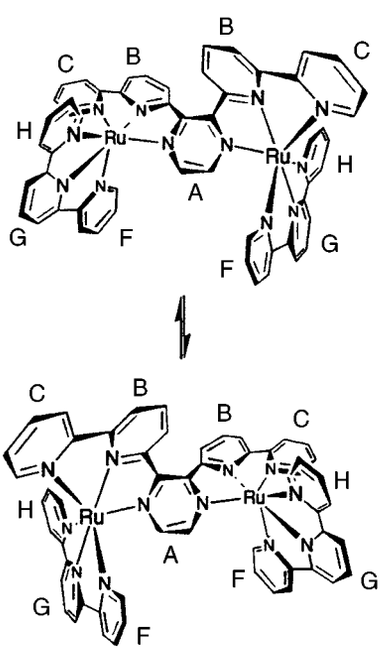

Fig. 6 Racemisation of diruthenium(II) complex **2**.

axis running through the pyrazine ring. Thus, in analogy to the racemisation process observed for purely organic helicenes,[3] the oscillation of the flanks of the terpy ring system between two chemically distinct environments, which occurs concomitant to the rocking of the bpy ligand fragments, would explain the observed dynamic phenomenon. Furthermore, models indicated a distance of *ca.* 3.9 Å between H(6^H) and H(3^B) on the

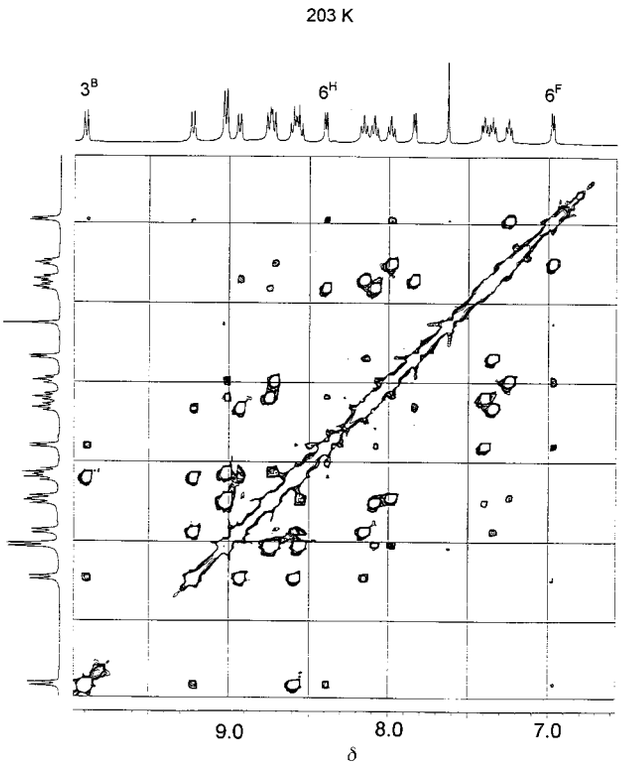

Fig. 7 The 400 MHz ^{1}H NMR phase-sensitive 2-D NOESY spectrum of complex **2** in $(CD_3)_2CO$ at 203 K. See text for explanation.

opposite side of the dimetallic complex. This relative closeness should be borne out by a distinctly stronger deshielding environment for H(6^H) than for H(6^F); the same arguments apply, but to increasingly lesser extents, to the 5-, 4- and 3-position hydrogens of the "F" and "H" rings, and the 3- and 5-position hydrogens of ring "G". With regard to the relative significance of the interactions between the "B" and "H" rings *versus* those between equivalent "B" rings, the same arguments apply for **2** as for **1**; terpy ring systems are sensitive spectators for the dynamic interactions of the "B" rings.

Evidence for this lowered symmetry of complex **2** in solution was garnered from a low-temperature 2-D NOESY experiment. At 203 K (Fig. 7) **2** exhibited 23 NOE interactions plus two exchange interactions in the form of cross-peak signals. The strong NOEs included intra-ring *ortho* and *meta* interactions (*e.g.* 3^B–4^B, 3^B–5^B, *etc.*), adjacent-ring interactions (*e.g.* short range 5^B–3^C, 5^G–3^H, *etc.*, and long range 5^B–4^C, 5^G–4^H, *etc.*) and, most significantly, the predicted interaction between H(6^H) and H(3^B). In the event of a chiral structure, H(3^B) will be significantly closer to H(6^H) in the *opposite* half of the complex than to H(6^F/6^H) in the *same* half (see later). Thus, the absence of any other significant bpy–terpy NOE interactions implies that the hydrogen pairs 3^B and 6^H in opposite halves of the complex are in close proximity and that **2** exists in a chiral, twisted geometry.

In the foregoing experiment we note that the two pairs of exchange cross peaks [*viz.* H(6^F/6^H) and H(4^F/4^H)] and *all* pairs of NOE cross peaks had the same phase as that of the diagonal signals. This is somewhat unexpected as NOE cross peaks for molecules in the extreme narrowing regime have opposite phase to that of diagonal peaks.[24] This implies that complex **2** is sufficiently large and bulky *not* to satisfy the rapid molecular tumbling criterion in low temperature solutions (*viz.* 203 K), so that the phase of its NOE cross peaks changes as a result of the dominance of zero-quantum relaxation pathways.[25] This was confirmed by NOE-difference spectra which showed negative enhancements normally observed with macromolecular species.

In order to measure the activation parameters for this process in complex **2**, bandshape analyses were performed on the signal pairs H(6^F/6^H) and H(5^F/5^H) (Fig. 8). Use of both spectral

Table 5 Kinetic data for the racemisation process in complex **2**

	k/s^{-1}	
T/K	$6^F/6^H$ region	$5^F/5^H$ region
243	15 ± 1	12.0 ± 0.5
253	70 ± 5	70 ± 2
263	190 ± 10	155 ± 5
273	[a]	410 ± 10
283	[a]	1500 ± 50
303	6250 ± 250	
313	14250 ± 750	
323	25000 ± 1000	

[a] Band too broad for fitting.

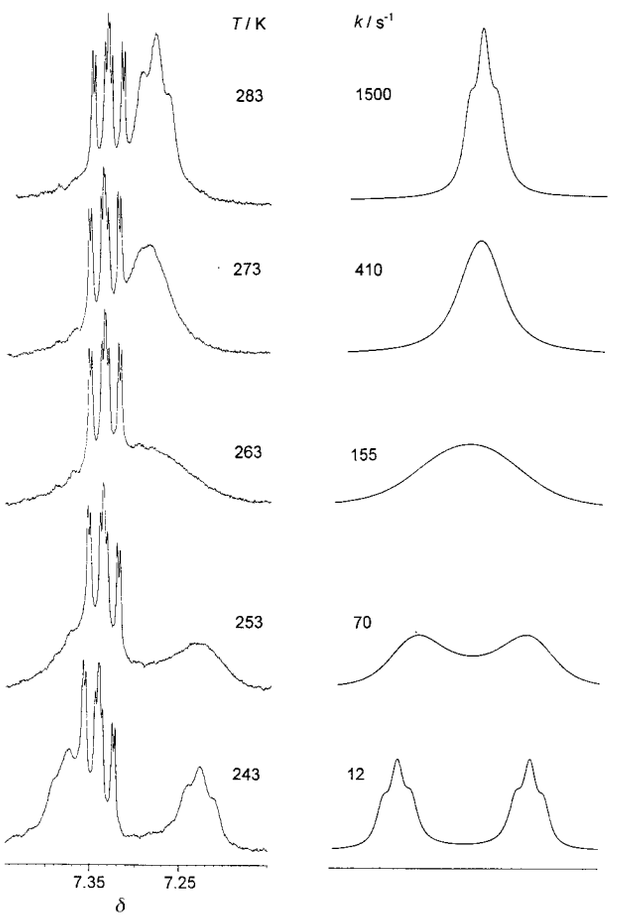

Fig. 8 Bandshape analyses of signals $H(5^F)$ and $H(5^H)$ of complex **2**, showing the best-fit rate constants. The spectator multiplet of $H(5^C)$ is also visible in the experimental spectra.

regions allowed for the evaluation of the associated rate constant, k, over a wider temperature range, values ranging from 15 to 2.5×10^4 s^{-1} being consequently determined (Table 5). Good agreement was achieved between experimental and computer simulated shapes and the fittings for signals of $H(5^F/5^H)$ are shown in Fig. 8. Activation energy data were calculated in the usual way and are included in Table 3.

The NMR spectroscopic data for complex **2** provide no direct insight into the nature of the mechanism for this process. However, the energy barrier ($\Delta H^{\ddagger}$) determined, 56.1 kJ mol^{-1}, is qualitatively consistent with the behaviour of the structurally analogous dithiophenopentahelicene **IV**, whose enantiomeric stability does not suffice for detection of optical rotation at room temperature.[26] In the ground state of purely organic helicenes possessing C_2 symmetry, C_s symmetry is expected for the transition state of racemisation.[4] Although this cannot be ruled out for **2**, the relatively low energy barrier also supports a mechanism in which the steric interaction of the pyridine "B" rings is avoided by either an appropriate distortion from regular octahedral co-ordination at the metallic centres or a twist-boat conformational deformation of the pyrazine ring. The relatively small magnitude of the entropy of activation ($\Delta S^{\ddagger}$) for the process rules out racemisation *via* a bond-breaking process.

Crystal structure studies

All the foregoing work alluded to a significant structural perturbation in complex **2**, and thus it was desirable to compare those results to its crystal structure. However, **2** was extremely reluctant to crystallise. Over many attempts using freshly prepared and freshly purified **2** with a variety of solvent mixtures, only non-crystalline material or single crystals which contained poorly ordered solvent molecules (*e.g.* acetone or acetonitrile) and which were too fragile to be manipulated could be isolated (see Experimental section).

The results of the most satisfactory measurement are depicted below (Fig. 9). Although rigorously asymmetrical, the complex possesses a nominal C_2 axis in the plane of the pyrazine ring and between the pyridine "B" rings; bond lengths and angles for both halves of the molecule are very similar (see Table 6). In particular, comparisons of the normal bond angles between the two differing ligand domains [*e.g.* $N(1^A)$–Ru–$N(1^F)$ to $N(1^A)$–Ru–$N(1^H)$, *etc.*] and the bite angle spanning both N_3-binding domains [$N(1^B)$–Ru-$N(1^G)$] both reflect a minor angular displacement of the terpy ring system to either side of the mean plane of the pyrazine ring. An angle of *ca.* 48° exists between the mean planes of the "B" rings. The non-bonding distance between opposing pairs of atoms $C(3^A)$ is 3.07 Å, which corresponds to through-space H · · · H separations of *ca.* 2.4 Å. The mean planes of the terpy ring systems are deflected by *ca.* 18° from being perfectly parallel, and non-bonding distances between opposing atom pairs here vary between 6.8 and 8.5 Å. Of further relevance to the through-space ^1H NMR spectroscopic effects are the observed non-bonding distances between $H(3^B)$ and $H(6^F/6^H)$, 5.9/3.9 Å. Thus, this helical twisting is very consistent with both the ^1H and ^{13}C NMR spectroscopic observations. At ambient temperatures both types of spectra can be fully rationalised in terms of a symmetry-averaged crystal structure but at lower temperatures the solid-state symmetry is also retained in solution.

The geometry of compound **I** forces strong steric interactions upon the "B" rings of the bpy units in complexes **1** and **2**. This induces remarkably similar dynamic processes in both complexes. In **1** the uncomplexed bpy group avoids contact with the relatively inflexible, Ru^{II}-binding bpy flank by rotating out of their common plane. This motion induces deshielding interactions between the pendant bpy and the side of the terpy ring lying *away* from it. In uniformly rigid dimetallic **2** a highly energetically disfavoured coplanar orientation of the bpy "B" rings can only be avoided by a mutual twisting of these units, resulting in a helicene-like structure. The protons of the opposite terpy which lie *in* the direction of this motion thereby experience strong deshielding from the bpy. For **1**, enantiomeric atropisomers and for **2**, right- and left-handed (*P*/*M*)[27] helicene-like complexes are produced, for which the activation parameters to racemisation have been determined. The magnitudes of the energy barriers ($\Delta H^{\ddagger}$) are, however, not great enough to allow for the isolation of optically active material at room temperature. Nevertheless, the electronic spectra and the electrochemical behaviour of both complexes indicate that for **2** moderate delocalisation of electron density over the scaffolding of **I** is possible.

Experimental

Materials and methods

Infrared spectra were recorded on Mattson Genesis Fourier-transform spectrophotometers with samples in compressed

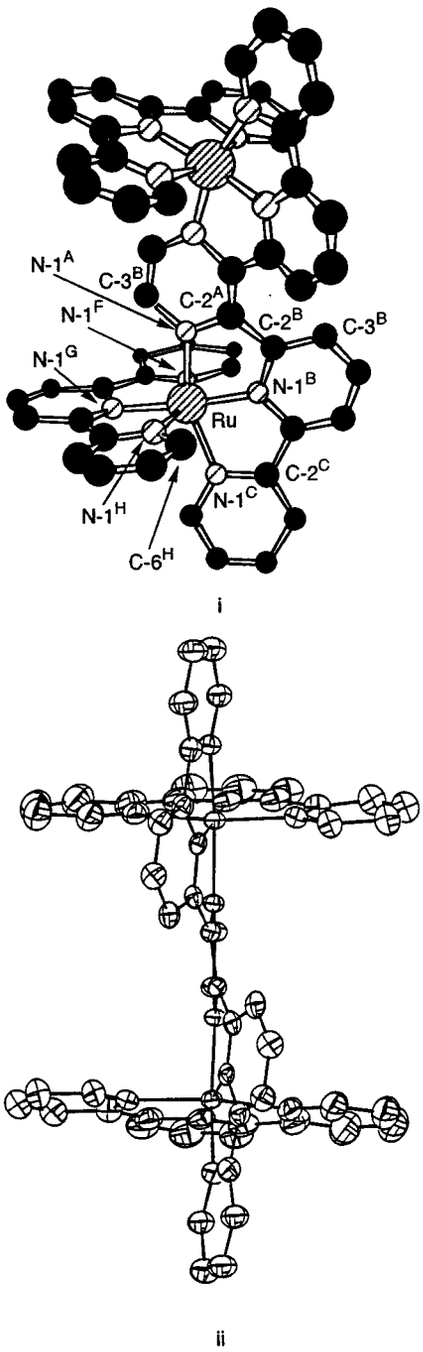

Fig. 9 Crystal structure of complex **2**: i, perpendicular to the Ru–Ru axis; ii, thermal ellipsoid presentation as seen along the C_2 axis bisecting the pyrazine ring. Hydrogen atoms, PF_6 counter ions and solvate molecules omitted for clarity.

KBr discs, proton NMR spectra on Varian Gemini (300 MHz) or Bruker DRX (400 MHz) spectrometers and carbon-13 NMR spectra on the same spectrometers at 75 and 100.6 MHz, respectively. All NMR spectra were recorded on $(CD_3)_2CO$ solutions at various temperatures using the Bruker B-VT 2000 temperature controller unit. Two-dimensional homonuclear-correlated COSY and NOESY spectra were obtained using the Bruker Avance version programs COSY 45 and NOESYTP. The ^1H–^{13}C correlated spectra (HMQC[20] and HMBC[21]) were recorded with the programs INVBTP and INV4LPLRND respectively. Rate data were based on total bandshape analysis of chosen ^1H spectral regions using the authors' version of the standard DNMR 3 program.[28] Fast atom bombardment (FAB) spectra were recorded on a Finnigan 8430 spectrometer using acetonitrile as a solvent and 3-nitrobenzyl alcohol as supporting matrix and the mass value for the most intense signal of an isotopomeric cluster is given. Time of flight MALDI (matrix assisted laser desorption ionisation) spectra were recorded using a PerSeptive Biosystems Voyager-RP Biospectrometry Workstation using 2,4,6-trihydroxyacetophenone as matrix in 1:1 acetronitrile–water solvent mixtures. Electrochemical measurements were performed with an Eco Chemie Autolab PGSTAT 20 system using glassy carbon working and platinum auxiliary electrodes with an Ag–AgCl electrode as reference. The experiments were conducted at 20 mV min^{-1} in purified acetonitrile containing 0.1 M [*n*-Bu_4N][PF_6] as supporting electrolyte. Ferrocene was added at the end of each experiment as an internal reference. Column chromatography was performed with aluminium oxide (activity III, Fluka). Compound **I** was prepared according to ref. 7.

Preparations

Complex 1. A mixture of 100 mg (0.26 mmol) **I**, 126 mg (0.29 mmol) terpyridineruthenium trichloride and 2.0 mL (16 mmol) *N*-ethylmorpholine in 3 mL ethanol was heated under reflux conditions for 4 h. Volatile material was removed by rotary evaporation under reduced pressure and vacuum (10 mbar). The residual material was dissolved in 20 mL acetonitrile, and treated with a solution of 3.0 g [NH_4][PF_6] in *ca*. 15 mL water. This mixture was concentrated by rotary evaporation under reduced pressure to complete precipitation of the crude product, which was separated from green Ru^{III}-containing impurities and purified by column chromatography (1:1 acetonitrile–toluene). This material was dissolved in acetonitrile and stirred for *ca*. 1 h with powdered calcium oxide, filtered through Celite and recrystallised from an acetonitrile–diisopropyl ether mixture to give 43 mg (16%) red prisms. In a similar experiment the initial fraction from the column was concentrated under vacuum, dissolved in dichloromethane and passed through aluminium oxide (activity III) to give, after removal of solvent, a 27% recovery of **I**. For **1**: IR (KBr) *v* 1602w, 1558w, 1450m, 1379w, 1243w, 847s, 767m and 557m cm^{-1}; TOF-MS *m*/*z* (relative intensity) = 724.5, [**I** + Ru(terpy)]$^+$, 100; 491.2 [**I** + Ru]$^+$, 34% (Found: C, 46.09; H, 2.90; N, 12.84. Calc. for $C_{39}H_{27}F_{12}N_9P_2Ru$: C, 46.26; H, 2.69; N, 12.45%).

Complex 2. A mixture of 69 mg (0.16 mmol) terpyridine ruthenium trichloride and 290 mg (1.6 mmol) silver tetrafluoroborate in 6 mL of acetone, which had been degassed with N_2, was heated for 3 h under reflux conditions under N_2 and with exclusion of light. After cooling to 25 °C the reaction mixture was filtered through a sintered glass frit, washed with 20 mL acetone, the solvent removed by rotary evaporation under reduced pressure below 45 °C and the remaining material dried at 0.1 mbar for 20 min. The residue was dissolved in 20 mL degassed *n*-butanol, combined with a solution of 27 mg (0.068 mmol) **I** in 5 mL *n*-butanol and heated under reflux conditions for 12 h under N_2. After solvent removal by rotary evaporation, the residual material was dissolved in 15 mL acetonitrile, filtered through a sintered glass frit and treated with a solution of 0.80 g [NH_4][PF_6] in *ca*. 30 mL water. This solution was concentrated under vacuum to complete precipitation of the crude product. After collecting by filtration, washing with water (20 mL) and drying at 200 mbar over P_2O_5, the crude product was purified by column chromatography (3:1 acetonitrile–toluene) and recrystallisation (acetronitrile–diisopropyl ether) to give 46 mg (34%) of purple prisms. IR (KBr): *v* 1450w, 841s, 768 and 557 cm^{-1} FAB-MS: *m*/*z* (relative intensity) = 1493 [{**I** + $Ru_2(terpy)_2$}$(PF_6)_3$]$^+$, 2; 1349 [**I** + $Ru_2(terpy)_2(PF_6)_2$]$^+$, 5; 1201 [**I** + $Ru_2(terpy)_2(PF_6)$]$^+$, 3% (Found: C, 39.52; H, 2.48; N, 10.40. Calc. for $C_{54}H_{38}F_{24}N_{12}P_4Ru_2$: C, 39.62; H, 2.34; N, 10.27%).

Crystallography

Details are compiled in Table 7. Data collection, structure solu-

Table 6 Selected bond lengths (Å) and angles (°) from the crystal structure of complex **2**

	[a]	[b]		[a]	[b]
$N(1^A)$–Ru	2.02(1)	2.04(1)	$N(1^F)$–Ru	2.09(1)	2.04(1)
$N(1^B)$–Ru	1.99(1)	1.95(1)	$N(1^G)$–Ru	1.98(1)	1.97(1)
$N(1^C)$–Ru	2.05(1)	2.08(1)	$N(1^H)$–Ru	2.09(1)	2.10(1)
$N(1^A)$–Ru–$N(1^B)$	78.4(4)	79.0(4)	$N(1^B)$–Ru–$N(1^H)$	103.7(4)	103.7(5)
$N(1^A)$–Ru–$N(1^C)$	159.1(4)	158.5(4)	$N(1^C)$–Ru–$N(1^F)$	91.0(5)	91.9(4)
$N(1^A)$–Ru–$N(1^F)$	92.0(4)	92.2(4)	$N(1^C)$–Ru–$N(1^G)$	103.8(5)	104.0(5)
$N(1^A)$–Ru–$N(1^G)$	97.1(4)	97.5(4)	$N(1^C)$–Ru–$N(1^H)$	92.6(5)	92.2(4)
$N(1^A)$–Ru–$N(1^H)$	92.4(4)	92.3(4)	$N(1^F)$–Ru–$N(1^G)$	78.1(5)	77.5(5)
$N(1^B)$–Ru–$N(1^C)$	80.7(4)	79.5(4)	$N(1^F)$–Ru–$N(1^H)$	157.9(5)	156.9(5)
$N(1^B)$–Ru–$N(1^F)$	98.4(4)	99.4(5)	$N(1^G)$–Ru–$N(1^H)$	79.9(5)	79.4(5)
$N(1^B)$–Ru–$N(1^G)$	174.3(5)	175.4(5)			

[a] Values for labelled side of molecule in Fig. 9. [b] Values for unlabelled side of molecule in Fig. 9

Table 7 Crystal data and parameters of data collection for complex **2**

Formula	$C_{70.50}H_{71}F_{24}N_{12}O_{5.50}P_4Ru_2$ $(C_{54}H_{38}N_{12}Ru_2{\cdot}4PF_6{\cdot}5.5C_3H_6O)$
M	1956.41
Crystal system	monoclinic
Space group	$P2/a$
a/Å	23.288(5)
b/Å	13.901(2)
c/Å	29.507(9)
β/°	108.70(3)
V/Å^3	9048(5)
Z	4
F(000)	3944
D_c/g cm^{-3}	1.44
Colour	Purple-red
μ/mm^{-1}	4.34
Crystal size/mm	0.25 × 0.40 × 0.75
T/K	223
Radiation (λ/Å)	Cu-Kα (1.54180)
No. measured reflections	11156
No. independent reflections	10561
No. reflections in refinement	6934
No. variables	1073
Final R	0.1145
Final R'	0.1293
Maximum, minimum in electron density difference map/e Å^{-3}	1.91, −1.38

tion and refinement presented various problems. The crystals contained solvent molecules from the crystallisation process and were very fragile. The sample chosen for data collection was protected with oil and fixed on an Enraf-Nonius CAD4 four circle diffractometer by freezing the oil drop using the Oxford CRYOstream cooling device. The usual corrections were applied. Absorption correction was determined using ψ scans. The structure was solved by direct methods using the program SIR 92.[29] Anisotropic least squares refinement was carried out on all non-H atoms using the program CRYSTALS[30] and Chebychev polynomial weighting.[31] Since the scan width of the reflections was broad (*ca*. 2.5°) the data did not give entirely satisfactory results. After having found all cations and anions, six acetone molecules were localised in the asymmetric unit, one of them on a special position (0.25, y, 0.50) of the space group $P2/a$. In the tetracation, the U values were restrained to meet the null motion criterion. The anions were refined, restraining the positions to the octagonal geometry. The localisable solvent molecules were restrained in a similar manner. Owing to the flat distribution of the electron density, disorder models for the solvent molecules were not used. High U values suggest, however, that some of these positions are nevertheless disordered due to thermal motion.

CCDC reference number 186/1284.

See http://www.rsc.org/suppdata/dt/1999/565/ for crystallographic files in .cif format.

Acknowledgements

We thank the companies Novartis AG, Biosynth AG and Shell Oil for chemical donations and the Treubel Fond for a stipend (F. R. H.). We are furthermore grateful to Professor E. C. Constable, Basel, Switzerland for encouraging this work and Dr. H.-M. Schiebel, Technische Universität Braunschweig, Germany for FAB-MS spectra.

References

1 A. E. Rowan and R. J. M. Nolte, *Angew. Chem.*, *Int. Ed. Engl.*, 1998, **37**, 63; C. Piguet, G. Bernardinelli and G. Hopfgartner, *Chem. Rev.*, 1997, **97**, 2005; E. C. Constable, *Tetrahedron*, 1992, **48**, 10013.

2 Y. Dai and T. J. Katz, *J. Org. Chem.*, 1997, **62**, 1274; A. M. Gilbert, T. J. Katz, W. E. Geiger, M. P. Robben and A. L. Rheingold, *J. Am. Chem. Soc.*, 1993, **115**, 3199.

3 W. H. Laarhoven and W. J. C. Prinsen, *Top. Curr. Chem.*, 1984, **125**, 63.

4 R. H. Janke, G. Haufe, E. U. Wurthwein and J. H. Borkent, *J. Am. Chem. Soc.*, 1996, **118**, 6031.

5 T. W. Bell and H. Jousselin, *Nature* (*London*), 1994, **367**, 441.

6 P. K.-K. Ho, K.-K. Cheung and C.-M. Che, *Chem. Commun.*, 1996, 1197.

7 F. R. Heirtzler, M. Neuburger, M. Zehnder and E. C. Constable, *Liebigs Ann./Recueil*, 1997, 297.

8 F. Heirtzler and T. Weyhermüller, *J. Chem. Soc.*, *Dalton Trans.*, 1997, 3653; T. Bark, T. Weyhermüller and F. Heirtzler, *Chem. Commun.*, 1998, 1475.

9 C. H. Braunstein, A. D. Baker, T. C. Streakas and H. D. Gafney, *Inorg. Chem.*, 1984, **23**, 857.

10 B. Gloaguen and D. Astruc, *J. Am. Chem. Soc.*, 1990, **112**, 4607; M. T. Ashby, G. N. Govindan and A. K. Grafton, *J. Am. Chem. Soc.*, 1994, **116**, 4801.

11 E. C. Constable and A. M. W. Cargill Thompson, *J. Chem. Soc.*, *Chem. Commun.*, 1992, 617.

12 G. S. Hanan, C. R. Arana, J.-M. Lehn, G. Baum and D. Fenske, *Chem.-Eur. J.*, 1996, **2**, 1292.

13 C. Arana and H. D. Abruña, *Inorg. Chem.*, 1993, **32**, 194.

14 P. Ford, F. P. De Rudd, R. Gaunder and H. Taube, *J. Am. Chem. Soc.*, 1968, **90**, 1187.

15 F. Barigelletti, L. Flamigni, V. Balzani, J.-P. Collin, J.-P. Sauvage, A. Sour, E. C. Constable and A. M. W. Cargill Thompson, *J. Am. Chem. Soc.*, 1994, **116**, 7692.

16 S. Ernst, V. Kasack and W. Kaim, *Inorg. Chem.*, 1988, **27**, 1146.

17 K. Nakamoto, *J. Phys. Chem.*, 1960, **64**, 1420.

18 *Handbook Series in Organic Electrochemistry*, eds. L. Meites and P. Zumann, CRC Press, Boca Raton, FL, 1977–1982, vols. I–V.

19 G. Denti, S. Campagna, L. Sabatino, S. Serrni, M. Ciano and V. Balzani, *Inorg. Chem.*, 1990, **29**, 4750.

20 A. Bax and S. Subramanian, *J. Magn. Reson.*, 1986, **67**, 565.

21 A. Bax and M. F. Summers, *J. Am. Chem. Soc.*, 1986, **108**, 2093.

22 A. Gelling, K. G. Orrell, A. G. Osborne and V. Sik, *J. Chem. Soc.*, *Dalton Trans.*, 1998, 937; E. W. Abel, V. S. Dimitrov, N. J. Long, K. G. Orrell, A. G. Osborne, V. Sik, M. B. Hursthouse and M. A. Mazid, *J. Chem. Soc.*, *Dalton Trans.*, 1993, 291; E. W. Abel, K. G. Orrell, A. G. Osborne, H. M. Pain, V. Sik, M. B. Hursthouse and K. M. A. Malik, *J. Chem. Soc.*, *Dalton Trans.*, 1994, 3441.

23 E. W. Abel, V. S. Dimitrov, N. J. Long, K. G. Orrell, A. G. Osborne, A. G. H. M. Pain, V. Sik, M. B. Hursthouse and M. A. Mazid, *J. Chem. Soc.*, *Dalton Trans.*, 1993, 597.
24 H. Kessler, M. Gehrke and C. Griesinger, *Angew. Chem.*, *Int. Ed. Engl.*, 1988, **27**, 490.
25 H. Günther, *NMR Spectroscopy*, Wiley, Chichester, 2nd edn., 1995, ch. 10.
26 M. B. Groen, H. Schadenberg and H. Wynberg, *J. Org. Chem.*, 1971, **36**, 2797.
27 R. Cahn, C. Ingold and V. Prelog, *Angew. Chem.*, *Int. Ed. Engl.*, 1966, **5**, 385.
28 D. A. Kleier and G. Binsch, DNMR 3 Program 165, Quantum Chemistry Program Exchange, Indiana University, IN, 1970.
29 A. Altomare, G. Cascarano, G. Giacovazzo, A. Guagliardi, M. C. Burla, G. Polidori and M. Camalli, *J. Appl. Crystallogr.*, 1994, **27**, 435.
30 D. J. Watkin, R. J. Carruthers and P. Betteridge, CRYSTALS, Chemical Crystallography Laboratory, Oxford, 1985.
31 J. R. Carruthers and D. J. Watkin, *Acta Crystallogr.*, *Sect. A*, 1979, **35**, 698.

Paper 8/07970F